Pure Appl. Chem., Vol. 71, No. 10, pp. 1871–1877, 1999.
Printed in Great Britain.

Generation and growth of nanoparticles in low-pressure plasmas*

U. R. Kortshagen[1,†], U. V. Bhandarkar[1], M. T. Swihart[2] and S. L. Girshick[1]

[1]*University of Minnesota, Dept. of Mechanical Engineering, 111 Church street SE, Minneapolis, MN 55455, USA;* [2]*SUNY Buffalo, Dept. of Chemical Engineering, Buffalo, NY 14260, USA*

Abstract: This invited talk focuses on two aspects of generation and growth of nanometer-sized particles in chemically active low-pressure plasmas: the nucleation of initial clusters and the subsequent growth due to coagulation of primary particles. Progress on the modeling of these processes is presented.

INTRODUCTION

Nanoparticle formation in low-pressure nonthermal plasmas is of interest from (at least) two seemingly opposite points of view. Nanoparticles unintentionally generated during plasma processing of microelectronic devices can produce so called 'killer defects' when they deposit on the wafer during processing. Since the feature size of microelectronic devices will decrease to about 50 nm over the next 12 years, a particle as small as 20 nm in diameter will be able to produce a 'killer defect' making nanoparticle contamination a much more severe problem than at present. Hence research on particle formation in plasmas has previously mainly focused on controlling and avoiding contaminant particle formation. However, more recently the scope of interest has broadened since a number of interesting, beneficial properties of nanometer-particles produced in plasmas has been found. It is believed that nanoparticles embedded into thin films bear potential for use in high-efficiency thin-film solar cells [1], nanocrystalline electronic memory devices [2], and photoluminescent silicon films, which are of high interest for new developments in optoelectronics.

The understanding of nanoparticle generation and growth is important for both these aspects since it might aid in generating 'good' nanoparticles with controlled properties as well as in avoiding 'killer' particle contamination in semiconductor manufacturing processes. Even though intense research on nanoparticle formation has been conducted over the past decade the main mechanisms of particle generation and growth are only poorly understood. Experiments conducted in SiH_4 plasmas have led to a three phase picture of the particle growth in some PECVD (Plasma Enhanced Chemical Vapour Deposition) processes [3,4]. During the first phase of about 100 ms initial spherical crystallites nucleate within the plasma and grow to a diameter of about 2 nm, which corresponds to several hundred atoms per particle. Once the particles have reached this size, a phase of rapid particle growth by coagulation of the primary particles sets in. The coagulation phase prevails for about 5 s and the particles grow to a size of about 50–60 nm in diameter. When the particles have reached this size, the coagulation process stops and particles continue to grow by molecular sticking of SiH_x clusters (third phase). During the entire process the particle size distribution remains rather monodisperse. Moreover, dramatic changes of the plasma properties during coagulation have been observed.

*Lecture presented at the 14th International Symposium on Plasma Chemistry, Prague, Czech Republic, 2–6 August 1999, pp. 1809–1918.
†*Corresponding author*: E-mail: uk@me.umu.edu

The goal of our work is to develop a comprehensive model which will describe particle nucleation, growth, and transport coupled to a self-consistent plasma model. In this paper we report progress on the modeling of the first phase, the nucleation phase, and the second phase, the coagulation phase. Even though the models presented are not yet combined in one self-consistent and comprehensive model, they already allow us to draw several interesting conclusions.

NUCLEATION MODELING

Our current clustering mechanism is based on a chemistry model for the neutral clustering of silicon hydrides in silane thermal CVD by Swihart & Girshick [5]. This model predicts that the higher silicon hydrides are predominately ring-structured, which implies that clusters are increasingly dehydrogenated. Using *ab initio* calculations and group additivity rules, Swihart & Girshick predicted thermodynamic properties of a large set of higher silanes with up to 10 silicon atoms. They then extrapolated reaction rate parameters known for the smaller silanes to predict the reaction rates for larger silanes. Silicon hydride clusters with more than 10 silicon atoms were considered to be *particles* and they were assumed to be formed irreversibly.

We have complemented the thermal chemistry by an extensive set of plasma-chemical reactions. The group of silyl radicals—not included in the thermal mechanism—was introduced, as well as negatively charged silicon hydrides, which are thought to be important in the clustering in plasmas. Thermochemical data were determined by group additivity, electron affinities via *ab initio* calculations. Estimates of rate coefficients are based mainly on the data compiled by Perrin *et al* [6]. In this compilation, mainly information for reactions of silane and disilane species can be found. For larger silicon hydrides extrapolations based on these data have been used. Details on these extrapolations will be presented in a forthcoming publication. For most ion-neutral reactions Langevin rates were used. The plasma chemical reactions included in our mechanism are:

Electron-impact dissociation of silane

$$SiH_4 + e \rightarrow SiH_3 + H + e$$
$$SiH_4 + e \rightarrow SiH_2 + 2H + e$$

Electron-impact dissociation of hydrogen

$$H_2 + e \rightarrow 2H + e$$

Electron-impact dissociation of higher silanes (38 reactions)

$$\text{Linear silane} + e \rightarrow \text{silyl} + \text{silylene} + H + e$$
$$\text{cyclic silane} + e \rightarrow H + \text{silyl} + e$$

Dissociative attachment of silane

$$SiH_4 + e \rightarrow SiH_3^- + H$$
$$SiH_4 + e \rightarrow SiH_2^- + 2H$$

Electron attachment to silicon hydrides (196 reactions)

$$Si_nH_m + e \rightarrow Si_nH_m^-$$

Silyl formation through H abstraction (36 reactions)

$$H + Si_nH_{2m} \rightleftharpoons Si_nH_{2m-1} + H_2$$

Neutralization/Recombination (196 reactions)

$$Si_nH_m^- + SiH_3^+ \rightarrow Si_nH_m + SiH_3 \ (n \leq 3)$$
$$Si_nH_m^- + SiH_3^+ \rightarrow Si_{n+1}H_{m+3} \ (n \geq 4)$$

Negative silylene/silyl charge exchange (1330 reactions)

$$Si_nH_{2m}B^- + Si_jH_{2k-1} \rightleftharpoons Si_nH_{2m}B + Si_jH_{2k-1}^-$$

Silylene-silane ion-molecule reaction with H_2 elimination (209 reactions)

$$Si_nH_{2m}B^- + Si_jH_{2k} \rightleftharpoons Si_{n+j}H_{2m+2k}B^- + H_2$$

Silylene-silylene ion-molecule reaction with H_2 elimination (192 reactions)

$$Si_nH_{2m}B^- + Si_jH_{2k}B \rightleftharpoons Si_{n+j}H_{2m+2k-2}B^- + H_2$$

Silyl-silane ion-molecule reaction with H_2 elimination (570 reactions)

$$Si_nH^-_{2m-1} + Si_jH_{2k} \rightleftharpoons Si_{n+j}H^-_{2m+2k-3} + H_2$$

Silyl-silane ion-molecule reaction with H_2 elimination (531 reactions)

$$Si_nH^-_{2m-1} + Si_jH_{2k}B \rightleftharpoons Si_{n+j}H^-_{2m+2k-3} + H_2$$

Silyl-silyl ion-molecule reaction with H_2 elimination (217 reactions)

$$Si_nH^-_{2m-1} + Si_jH_{2k-1} \rightleftharpoons Si_{n+j}H_{2m+2k-4}B^- + H_2$$

The notation Si_xH_yB is used to distinguish the silylene di-radical from its silene isomer species Si_xH_yA with no unpaired electrons. The clustering model is currently a zero-dimentional model, i.e. spatial non-uniformities of the plasma and species concentrations are neglected. However, we felt that it is important to include diffusion as a loss mechanism in our clustering model. Hence we chose to approximately include diffusion in the form of an irreversible reaction ('film formation') with a rate constant equal to the diffusion frequency D/Λ^2. The diffusion coefficients D were computed following [7] assuming that the species considered diffuses in the silane background gas. For Λ a typical diffusion length of 1 cm was assumed. Since negative clusters are confined by the space charge field diffusion does not contribute to their loss. The lifetime of anions is thus determined by the time for neutralization with positive ions.

Currently we use the positive ion concentration, the silane concentration and the gas temperature as input parameters, which are held constant during the simulation. The positive ion concentration can be considered as a measure for the RF power applied to the reactor. We also assume that SiH_3^+ is the only positive ion species. The electron density and temperature are variable throughout the simulation. The electron density is determined from the plasma-quasineutrality, the temperature from the requirement of a constant ionization rate. Chemical kinetics clustering calculations were performed with a zero-dimensional code based on the SENKIN code from the CHEMKIN code family [8], which was modified to include the inflow of silane gas into the reactor, the diffusion of species to the walls, and the variation of electron temperature and density.

Figure 1 shows a typical result of a clustering simulation for a plasma in pure silane. The positive ion density is $n_i = 3\times10^9\,cm^{-3}$, a value observed in many experiments. The pressure is 100 mTorr (13.3 Pa).

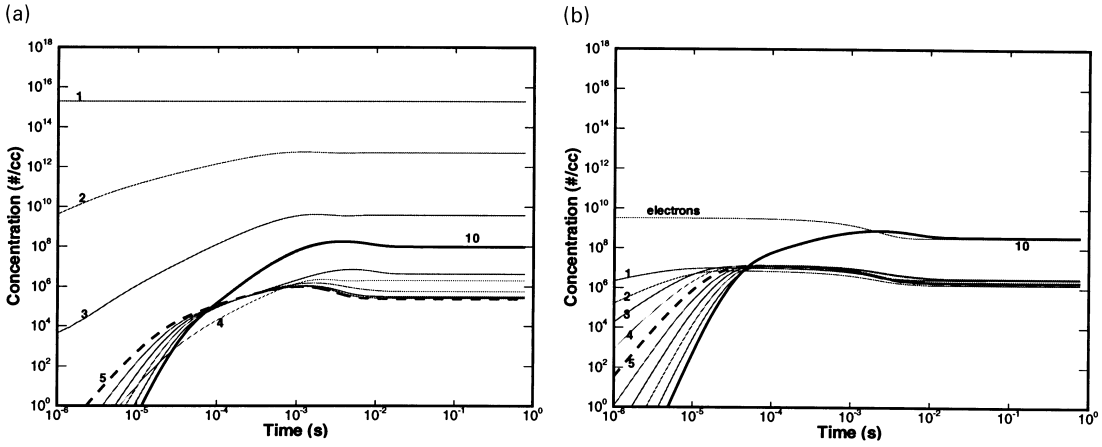

Fig. 1 Clustering of neutral silicon hydrides (a) and anionic silicon hydrides (b) for $n_i = 3\times10^9\,cm^{-3}$ and 100 mTorr and a gas temperature of 500 K. The numbers at the curves denote the number of Si atoms per cluster.

For these conditions negative clusters (anions) are more abundant than neutral clusters. We have observed that this trend reverses when higher positive ion densities (RF powers) are considered.

From our model we can draw three main conclusions:

1. At low plasma density (RF power density) anionic clustering is dominant. With increasing power density neutral clustering becomes more important and neutral clustering can finally become the dominant clustering pathway.
2. Increasing RF power density and gas temperature both favor the formation of cyclic or polycyclic silicon hydrides. This seems mainly related to an increased production in silylene di-radicals which can isomerise via ring formation.
3. The clustering rate depends more than linearly on the plasma density (RF power).

PARTICLE COAGULATION MODELING

We have developed a coagulation model for particles in low pressure plasmas which self-consistently accounts for changes in the plasma parameters and for the electrical charging of particles [9]. The coagulation of particles is described by a model based on the General Dynamic Equation (GDE) for an aerosol which describes the temporal evolution of the particle size distribution. The distribution of particles is usually considered in terms of volume v. If $n(v)$ denotes the number density of particles in the range $[v,v+dv]$ in a spatially uniform system, assuming that the total particle volume is constant, it is found by the equation:

$$\frac{\delta n(v)}{\delta t} = \frac{1}{2}\int_0^v \beta(v', v-v')n(v')n(v-v')dv' - \int_0^\infty \beta(v,v')n(v)n(v')dv'. \tag{1}$$

The first term for the right had side accounts for the gain of particles in the range $[v,v+dv]$ due to coagulation of smaller particles of any volume (size). The $\beta(v,v')$ term is the frequency of coagulation between particles of volume v and v'.

Coagulation of particles in plasmas is strongly modified by the electrical charge of the particles. The particle charge typically depends on the particle size as well as on the plasma parameters such as electron and ion densities and temperatures. Since particle charging is a stochastic process even particles of a given volume v will have a charge distribution function $F_k(v)$, where F_k denotes the fraction of particles of a size v which carry a charge $Z=ke$ with e the elementary charge and k an integer. Following Schweigert & Schweigert [10] we have developed a system of rate equations for the temporal change of the fraction F_k due to additional charging of particles with a charge state $k+1$ and $k-1$, respectively. The process leading to additional negative charging of a particle with the charge $(k+1)e$ is the capture of a plasma electron, which is described by a charging frequency ν_e^{k+1} given by the OML theory [11]. Processes leading to additional positive charging of particles carrying a charge $(k-1)e$ are capture of positive ions described by a frequency ν_i^{k-1} given by the OML theory, UV photo-detachment with a frequency ν_γ, secondary electron release due to energetic sheath electrons with a frequency ν_{se}, and electron release due to collisions with excited atoms with a frequency ν_{qu}. For more details the reader is referred to [9]. Assuming steady state of the charge distribution, a recursive formula for the charge distribution can be derived:

$$F_{k+1} = \frac{\nu_i^k + \nu_\gamma + \nu_{se} + \nu_{qu}}{\nu_e^{k+1}} F_k \tag{2}$$

The particle charge distribution obviously depends on a number of plasma parameters which have to be determined self-consistently during the simulation of the coagulation process. We use a 'global' zero-dimensional plasma model to find these parameters. While strictly speaking the entire set of parameters has to be found by the solution of the entire set of equations, in a simplified view one can associate certain parameters with certain equations which have the strongest influence on this parameter. For instance, the electron temperature is mainly determined by the ion balance equation

$$n_i \frac{D_a}{\Lambda} A_S + n_i \nu_{ap} V = n_e \nu_i(T_e) V, \tag{3}$$

with n_e the electron density, D_a the ambipolar diffusion coefficient, ν_{ap} the ion attachment frequency to particles, and $\nu_i(T_e)$ the ionization frequency. A_S is the electrode area and V the plasma volume.

The ion density is mostly determined by the RF power balance equation

$$P_{rf} = n_e(\nu_i u_i + \nu_{ex} u_{ex})V + n_i \frac{D_a}{\Lambda} A_s e V_{sh}, \tag{4}$$

with ν_i and ν_{ex} the frequencies for ionization and excitation for the background gas, and u_i and u_{ex} the respective threshold energies. The last term on the right hand side describes the power lost in ion acceleration in the sheath with V_{sh} the sheath voltage.

The electron density is found from the plasma quasineutrality equation

$$n_i = \overline{Z}(\overline{R_p}) n_p + n_e, \tag{5}$$

with $\overline{Z}(\overline{R_p})$ the average particle charge of particles with the average radius $\overline{R_p}$. (Here the approximation that $\overline{Z}(\overline{R_p})$ is equal to the average charge of the charge-size distribution has been used for reasons of numerical efficiency.) A corona type balance equation is used to find the densities of excited atomic states:

$$n_e \nu_{ex} = n_{ex} g A_{ij} \tag{6}$$

with n_{ex} the excited state density, g an escape factor, and A_{ij} the transition probability.

Figure 2 shows numerical results of our coagulation model for the concentration of particles and the mean particle radius. Initial conditions were chosen like those observed in the experiments by Bouchoule & Boufendi [4], i.e. we assume primary particles with a radius of 1 nm and a concentration of $2\times10^{12}\,\mathrm{cm}^{-3}$. After 1 s the particle concentration has decreased by about four orders of magnitude and the mean radius has increased to 20 nm. In comparison to the coagulation of a neutral aerosol (dash-dotted lines) it can be seen that coagulation in the plasma is initially enhanced. This is caused by the charge distribution of very small particles which has a certain fraction of positively as well as negatively charged particles. However, after about 1 s the coagulation of particles slows down noticeably and the coagulation of a neutral aerosol becomes faster. The reason for this is that particles have grown to such a size that all particles become negatively charged which suppresses coagulation. We have also studied the effect of changing the efficiency of UV photo-detachment from a quantum efficiency of 1.0 (full line) to 0.2 (dashed line). While this only seems to have a slight effect on the coagulation dynamics, our calculations show that it has a rather profound effect on the self-consistent plasma parameters. Depending on the efficiency of photo-detachment considered T_e ranges from about 3 eV at a quantum efficiency of 1.0 up to 8 eV at a quantum efficiency of 0.2. Electron densities are one and two orders of magnitude smaller than the positive ion densities, respectively.

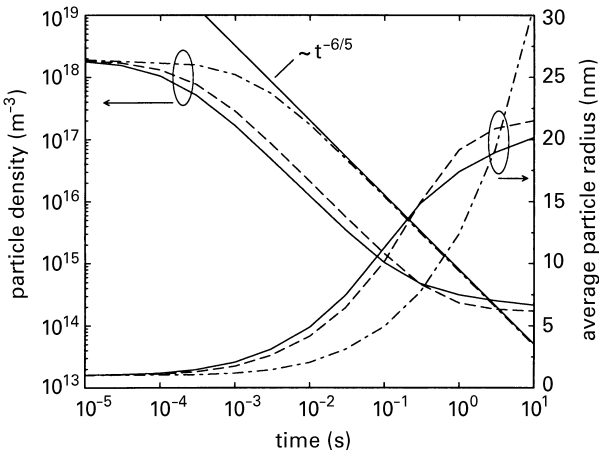

Fig. 2 Particle number density and average radius during coagulation. The full lines denote particle charging including UV photo-detachment, the dashed lines with reduced photo-detachment. The dash-dotted lines show the behaviour of a neutral aerosol.

Our model also gives some insight into the conditions necessary for coagulation to occur. In experiments it was observed that a certain minimum density of particles is necessary for coagulation to set in. In this respect it is instructive to study Fig. 3 which shows the coagulation dynamics of particles with a give initial density of $n_p = 2 \times 10^{12}\,\mathrm{cm}^{-3}$ and size of 2 nm for different values of RF power. It can be seen that the coagulation rate starts to significantly slow down as soon as the particle density has dropped to the value of the ion positive density as a consequence of the coagulation process. This is actually quite plausible, since it means that on average every particle can become singly negatively charged while still maintaining plasma quasineutrality. From this it can be concluded that coagulation would be mainly prevented if the initial particle density would be less than the positive ion density. In this sense the positive ion density can be considered as the critical density for the onset of particle coagulation.

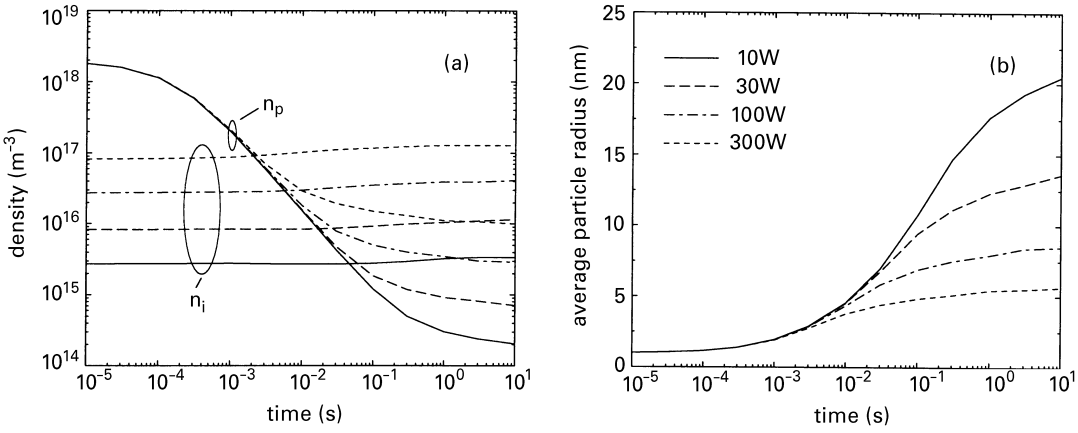

Fig. 3 Temporal evolution of (a) the particle density and the ion density and (b) the particle radius for different RF powers.

SUMMARY AND OUTLOOK

In this paper we have presented a chemical kinetics model which describes clustering in low-pressure silane plasmas and a model which describes particle growth due to coagulation. Both models are presently zero-dimensional and do not address spatial transport of species and plasma non-uniformities in a consistent manner. Main results of our clustering model are that anionic clustering dominates at low RF power densities while neutral clustering becomes more important at high power densities. Cyclic and polycyclic structures are formed particularly at high power densities and gas temperatures, and the clustering rate increases faster than linear with the power density. The coagulation model showed that coagulation of particles in plasmas is initially enhanced compared to an aerosol of neutral particles due to bipolar charge on the particles. In the later phase the particles become only negatively charged and coagulation is suppressed. The positive ion density corresponds to the critical density of initial particles for coagulation to occur.

The next step of our research will consist of the combination of these two models. The nucleation rate derived from the clustering model will be used as a source rate in our coagulation model. Both models will be extended to a one-dimensional geometry and combined with a more sophisticated plasma model. We hope that such a comprehensive model will enable us to make accurate predictions about the regions of particle formation in low-pressure silane plasmas.

ACKNOWLEDGEMENTS

This work was supported in part by NSF grant ECS-9731568 and by the University of Minnesota Supercomputing Institute.

REFERENCES

1 P. Roca i Cabarrocas, P. St'ahel, S. Hamma. Stable single junction p-i-n solar cells with efficiencies approaching 10%. In *2nd World Conference and Exhibition on Photovoltaic Solar Energy, Vienna, 6–10 July 1998* (1998).

2 S. Tiwari, F. Rana, K. Chan, Shi. Leathen, H. Hanafi. Single charge and confinement effects in nano-crystal memories. *Appl. Phys. Lett*. **69**, 1232–1234 (1996).

3 A. Bouchoule, L. Boufendi. Particulate formation and dusty plasma behaviour in argon-silane rf discharge. *Plasma Sources Sci. Technol*. **2**, 204 (1993).

4 L. Boufendi, A. Bouchoule. Particle nucleation and growth in a low-pressure argon-silane discharge. *Plasma Sources Sci. Technol*. **3**, 263 (1994).

5 M. T. Swihart, S. L. Girshick. Thermochemistry and kinetics of silicon hydride cluster formation during thermal decomposition of silane. *J. Phys. Chem. B*. **103**(1), 64–76 (1999).

6 J. Perrin, O. Leroy, M. C. Bordage. Cross-sections and rate constants and transport coefficients in silane plasma chemistry. *Contrib. Plasma Phys*. **36**(3), (1996).

7 R. C. Reid, J. M. Prausnitz, B. E. Poling. *The Properties of Gases and Liquids*. McGraw-Hill, New York (1987).

8 R. J. Kee, F. M. Rupley, J. A. Miller. Report no. sand87-8216. Unpublished technical report, Sandia National Laboratories, CA, USA. (1990).

9 U. Kortshagen, U. Bhandarkar. Modeling of particulate coagulation in low pressure plasmas. *Phys. Rev. E*. **60**(1), 887 (1999).

10 V. A. Schweigert, I. V. Schweigert. Coagulation in low-temperature plasmas. *J. Phys. D: Appl. Phys*. **29**, 655 (1996).

11 J. E. Allen. Probe theory—the orbital motion approach. *Physica Scripta*. **45**, 497 (1992).